Title page:

Sophocarpine attenuates wear particle-induced implant loosening by inhibiting osteoclastogenesis and bone resorption via suppression of the NF-κB signaling pathway in a rat model

Running title:

Sophocarpine impairs osteolysis via NF-κB

Chen-he Zhou[1,2,3], Zhong-li Shi[1,2], Jia-hong Meng[1,2], Bin Hu[1,2], Chen-chen Zhao[1,2], Yu-te Yang[1,2], Wei Yu[1,2], Ze-xin Chen[4], Boon Chin Heng[5], Virginia-Jeni Akila Parkman[3], Shuai Jiang[6], Han-xiao Zhu[1,2], Hao-bo Wu[1,2], Wei-liang Shen[1,2**], Shi-gui Yan[1,2,*]

1. Department of Orthopedic Surgery, Second Affiliated Hospital, School of Medicine, Zhejiang University, Hangzhou, People's Republic of China
2. Orthopedic Research Institute of Zhejiang University, Hangzhou, People's Republic of China.
3. Department of Oral Medicine, Infection and Immunity, Harvard School of Dental Medicine, Boston, Massachusetts, USA
4. Center of Clinical Epidemiology & Biostatistics, Department of Science and Education, the Second Affiliated Hospital, School of Medicine, Zhejiang University, Hangzhou, Zhejiang, China
5. Faculty of Dentistry, The University of Hong Kong, Pokfulam, Hong Kong
6. Department of Hand Surgery, the First Affiliated Hospital of Zhejiang University, Hangzhou, People's Republic of China

The first three authors contributed equally to this work

This article has been accepted for publication and undergone full peer review but has not been through the copyediting, typesetting, pagination and proofreading process which may lead to differences between this version and the Version of Record. Please cite this article as doi: 10.1111/bph.14092

*Corresponding author: Shigui Yan
Department of Orthopedic Surgery, 2nd Affiliated Hospital,
School of Medicine, Zhejiang University,
88 Jie Fang Road,
Hangzhou, 310009, China
Email: zrjwsj@zju.edu.cn Tel: +86-571-87783530

**Co-corresponding author: Wei-liang Shen
Department of Orthopedic Surgery, 2nd Affiliated Hospital,
School of Medicine, Zhejiang University,
88 Jie Fang Road,
Hangzhou, 310009, China
Email: wlshen@zju.edu.cn Tel: +86-571-89713669

Abstract

Background and Purpose

Aseptic prosthesis loosening, caused by wear particles, is one of the most common causes of arthroplasty failure. Extensive and over-activated osteoclast formation and physiological functioning are regarded as the mechanism of prosthesis loosening. Therapeutic modalities based on inhibiting osteoclast formation and bone resorption have been confirmed to be an effective way of preventing aseptic prosthesis loosening. In this study, we have investigated the effects of sophocarpine (SPC, derived from *Sophora flavescens*) on preventing implant loosening and further explored the underlying mechanisms.

Experimental Approach

The effects of SPC in inhibiting osteoclastogenesis and bone resorption were evaluated in RANKL-induced osteoclast formation in vitro. A rat femoral particle-induced peri-implant osteolysis model was established. Subsequently, micro-CT, histology, mechanical testing and bone turnover were used to assess the effects of SPC in preventing implant loosening.

Key Results

In vitro, we found that SPC suppressed osteoclast formation, bone resorption, F-actin ring formation and osteoclast-associated gene expression by inhibiting NF-κB signaling, specifically by targeting IκB kinases (IKKs). Our in vivo study showed that SPC prevented particle-induced prosthesis loosening by inhibiting osteoclast formation, resulting in reduced periprosthetic bone loss, diminished pseudomembrane formation, improved bone-implant contact, reduced bone resorption-related turnover, and enhanced stability of implants. Inhibition of NF-κB signaling by SPC was further confirmed in vivo.

Conclusion and Implications

Our data demonstrated that SPC can prevent implant loosening through inhibiting osteoclast formation and bone resorption. Thus,SPC might be a novel therapeutic agent to prevent prosthesis loosening and for osteolytic diseases.

Abbreviations

TJA: total joint arthroplasty; UHMWPE: ultra-high molecular weight polyethylene; PGE2: prostaglandin E2; M-CSF: macrophage colony-stimulating factor; RANKL: receptor activatior of nuclear factor κB ligand; NFATc1: nuclear factor of activated T cells c1; SPC: sophocarpine; α-MEM: alpha modification of Eagle's medium; IKKβ: IκB kinase β; TAK1: transforming grouth factors-β-activated kinase 1; CTX-1: type I collagen cross-linked C-terminal telopeptide; TRAP: tartrate-resistant acid phosphatase; PFA: paraformaldehyde; BMD: bone mineral density; ROI: region of interests; BV/TV: bone volume/ total volume; Conn.D: connective density; SMI: structural model index; Tb.N: trabecular number; Tb.Th: trabecular thickness; Tb.Sp: trabecular separation; BIC: bone-implant contact; B.Ar/T.Ar: bone area/total area; BMM: bone marrow-derived macrophage; RT: room temperature; SEM: scanning electron microscope; TBST: tris-buffered saline tween-20; ALP: alkaline phosphatase; ARS: Alizarin Red S; RUNX2: Runt-related transcription factor 2; OCN: osteocalcin; TLRs: toll like receptors; NO: nitric oxide.

Keywords

sophocarpine; implant-derived wear particle; implant loosening; osteoclast; NF-κB

Chemical compounds studied in this article

Sophocarpine (PubChem CID: 115269)

Introduction

Aseptic implant loosening is one of the most common complications of long-term total joint arthroplasty (TJA), which would eventually require a revision surgery. There were 38,310 hip and 16,711 knee revision surgeries performed in the UK due to aseptic loosening, between April 1, 2003 and December 31, 2015 (Porter, 2016). This is generally considered to be caused by an adverse response to implant-derived wear particles emanating from material components, including ultra-high molecular weight polyethylene (UHMWPE) and metal biomaterials (Jiang *et al.*, 2013; Gallo *et al.*, 2014; Pajarinen *et al.*, 2014). These wear particles stimulate the secretion of chemokines and pro-inflammatory cytokines, including TNF-α, IL-1β, IL-6, IL-11 and prostaglandin E2 (PGE 2), which may provoke a local inflammatory reaction that increases osteoclastogenesis and bone resorption, resulting in periprosthetic osteolysis, dense pseudomembrane formation and reduced implant fixation properties (Ingham *et al.*, 2005; Holt *et al.*, 2007; Purdue *et al.*, 2007; Athanasou, 2016). Therefore, a potential therapeutic strategy to prevent implant loosening is to suppress osteoclast over-formation and its functions.

Osteoclasts, originating from hematopoietic monocytes and macrophages, are fused multinucleated giant cells with the principal function of bone-resorption. The differentiation of osteoclasts require stimulation by macrophage colony-stimulating factor (M-CSF) and receptor activator of nuclear factor κB ligand (RANKL) (Kong *et al.*, 1999; Takahashi *et al.*, 2003), and involve activation of downstream signaling pathways, such as the MAPK and NF-κB signaling pathways (Pearson *et al.*, 2001; Takaesu *et al.*, 2001). This in turns further leads to the activation and up-regulation of two crucial transcription factors for osteoclast

formation, c-Fos and nuclear factor of activated T cells c1 (NFATc1) (Takayanagi *et al.*, 2002; Boyle *et al.*, 2003). The osteoclasts play their role in bone resorption through membrane polarization and the formation of an actin-rich sealing zone, which lead to the secretion of acids and proteolytic enzymes that dissolve and degrade the mineralized bone matrix (Boyle *et al.*, 2003; Jurdic *et al.*, 2006).

Due to the key role of osteoclasts in periprosthetic osteolysis and related implant loosening, drugs targeting the suppression of osteoclastic signaling pathways are found to be effective in preventing and treating the disorder. These include bisphosphonates, sclerostin antibody and strontium ranelate (Liu *et al.*, 2012b; Qu *et al.*, 2013; Liu *et al.*, 2014). Sophocarpine (SPC) (Figure 1A) is one of the major bioactive compounds derived from the natural plant *Sophora flavescens*, which is widely distributed in Russia, Japan, India and China. Anti-inflammatory, anti-tumor, anti-allergic, cardioprotective and neuroprotecive effects have been demonstrated in previous studies (Yang *et al.*, 2011; Yifeng *et al.*, 2011; Gao *et al.*, 2012; Wang *et al.*, 2012; Li *et al.*, 2014; Zhang *et al.*, 2016a). Researchers have shown that SPC can inhibit LPS-induced inflammation in RAW 264.7 cells via the NF-κB and MAPKs signaling pathways (Gao *et al.*, 2009; Gao *et al.*, 2012). Additionally, SPC's cardioprotective effects of this compound were reported in another study, which involved suppression of the NF-κB signaling pathway (Li *et al.*, 2011). However, little is known about the effects of SPC on osteoclasts and osteolytic-related diseases. As a result of the NF-κB and MAPKs signaling pathways role in osteoclast formation and SPC's suppressive effects on these signaling pathways in macrophages, we hypothesize that SPC may prevent particle-induced implant loosening by inhibiting osteoclast formation and functioning.

Our study showed that SPC attenuated osteoclast formation and function by suppressing the NF-κB signaling pathway in vitro, and its likely target might be the IκB kinase (IKKs). We further confirmed that SPC prevented particle-induced prosthesis loosening by inhibiting osteoclast formation via suppression of the NF-κB signaling pathway in vivo.

Materials and methods

Media and reagents

Alpha modification of Eagle's medium (α-MEM), FBS and penicillin/streptomycin were purchased from Gibco-BRL (Sydney, Australia). SPC, purchased from Selleck Chemicals (Houston, USA), was dissolved in DMSO, and stored at -20℃ in the dark, prior to being utilized in experiments. The Prime Script RT reagent kit and SYBR® *Premix Ex Taq*™ II were purchased from TaKaRa Biotechnology (Otsu, Shiga, Japan). The cell counting kit (CCK-8) was purchased from Dojindo Molecular Technology (Kumamoto, Japan). Recombinant human M-CSF and human RANKL were supplied by R&D systems (Minneapolis, MN). Specific primary antibodies against ERK (#4695), JNK (#9252), p38(#9212), IκBα (#4814), NF-κB p65(#8242), IκB kinase β (IKKβ)(#8943), phospho-ERK (Thr202/Tyr204)(#4370), phospho-JNK (Thr183/Tyr185)(#4668), phospho-p38 (Thr180/Tyr182)(#4511), phospho-IκBα (Ser32)(#2859), phospho-NF-κB p65 (Ser536)(#3033), phospho-IKKα/β (Ser176/180)(#2697), phospho-transforming growth factors-β-activated kinase 1 (TAK1)(#9339), TAK1(#5206) and α-Tubulin(#2144) were obtained from Cell Signaling Technology (Cambridge, MA, USA); specific primary antibodies against GAPDH (sc-20358), NFATc1(sc-7294), Cathepsin K(sc-48353), iNOS (sc-7271) and COX-2 (sc-166475) were obtained from Santa Cruz Biotechnology (Santa Cruz, CA, USA); primary antibody against active NF-κB-p65(MAB3026) was obtained from Millipore (Merck KGaA, Germany). HRP-conjugated secondary antibodies against rabbit IgG, mouse IgG and goat IgG were obtained from Santa Cruz Biotechnology (Santa Cruz, CA, USA). Bone slices and type I collagen cross-linked C-terminal telopeptide (CTX-1) were purchased from Immunodiagnostic Systems Limited (Boldon, UK). Commercial ELISA kits for rat PGE_2 was purchased from R&D systems (Minneapolis, MN, USA). Tris, glycine, sodium dodecyl sulfate (SDS), Rhodamine-conjugated phalloidin for F-actin staining, Diagnostic Acid Phosphatase kit for tartrate-resistant acid phosphatase (TRAP), DMSO, Griess reagent and all other reagents were obtained from Sigma-Aldrich (St. Louis, MO, USA)., unless stated otherwise.

Bone marrow-derived macrophage (BMM) culture and cell viability assay

Primary rat bone monocyte/macrophage precursors were isolated from the long bones of male SD rats weighing about 100g and cultured in α-MEM supplemented with 10% (v/v) FBS, 2mM L-glutamine, 100U/ml penicillin/streptomycin (complete α-MEM) and 30ng mL^{-1} M-CSF for 2 days to induce differentiation into BMMs. Cell culture was carried out within a 37°C humidified incubator containing 5% (v/v) CO_2, until cells were fully confluent. To explore the ratio of macrophage population in the whole cell population after 2 day culture, we collected the cells and analyzed using flow cytometry.

Cells were seeded into 96-well plates at a density of 2×10^4 cells/well for 24h, and subsequently treated with or without different dilutions of SPC (0.31-2mM) for 48h or 96h. Subsequently, the CCK-8 assay was used to assess the cytotoxic effects of SPC by adding 10μL of CCK-8 buffer into each well, and the plate was incubated for another 4 h. The OD was measured by using an ELX800 absorbance microplate reader (Bio-Tek Instr., Winooski, VT, USA) at a wavelength of 450 nm (650nm reference).

Osteoclast differentiation and TRAP staining

A cell count of 6×10^3 cells/well of BMMs were seeded into a 96-well plate with complete α-MEM containing 30ng mL^{-1} M-CSF, 50ng mL^{-1} RANKL and SPC (0, 0.25, 0.50, or 1.00 mM), followed by changes of culture media every 2 days for 5 days. Then, cells were fixed with 4% (w/v) paraformaldehyde (PFA) at 4°C for 30 min, washed twice with PBS, and stained with the TRAP staining kit according to the manufacturer's protocol. TRAP-positive cells with more than 3 nuclei were considered as mature osteoclasts, and their number and spread area were quantified under microscopy.

Immunofluorescence staining for F-actin ring formation

To observe F-actin ring formation, BMM were cultured on bovine bone slices with M-CSF and RANKL for 5 days, and were subsequently treated with serial dilutions of SPC (0, 0.25, 0.50, or 1.00 mM) for another 48h. The cells were then fixed in 4% (w/v) PFA for 30 min and subsequently permeabilized for 5 min with 0.2% (v/v) Triton X-100, followed by

being incubation with rhodamine-conjugated phalloidin diluted (1:100) in 0.2% (w/v) BSA-PBS for 1 h at room temperature (RT). Then the cells were stained with 4', 6-diamidino-2-phenylindole (KeyGen Biotech, Nanjing, China) for 5 min to visualize their nuclei and mounted with ProLong Gold anti-fade mounting medium (Invitrogen Life Technologies). Samples were analyzed and fluorescence images were captured using a NIKON A1Si spectral detector confocal system equipped with 40×(dry) lenses. Five wells were randomly chosen in each group to calculate the number and size of the F-actin ring cells by using the Image J software.

Bone resorption pit assay

BMM cells were treated with 30 ng mL^{-1} M-CSF and 50 ng^{-1} mL RANKL for 4 days. Equal numbers of osteoclasts were seeded overnight on bovine bone slices in 96-well plates. Cells were then cultured in complete α-MEM containing 30 ng mL^{-1} M-CSF, and 50 ng^{-1} mL RANKL with different dosages of SPC (0, 0.25, 0.50, or 1.00 mM) for another 48h. Cells were gently removed by mechanical agitation, and resorption pits were observed under a scanning electron microscope (SEM) (S-4800, Hitachi, Japan). Five random fields per bone slice were selected for quantitative analysis and independent experiments were repeated at least five times. The area of bone resorption was quantified using Image J software.

Cell culture, RNA isolation and quantitative PCR

To detect the effects of SPC on osteoclast formation and functions, BMM cells were seeded at a density of 10×10^4 cells/well in 6-well plates and cultured in osteoclastogenic medium (complete α-MEM containing 30ng mL^{-1} M-CSF and 50ng mL^{-1} RANKL) with different ways of SPC treatment. To detect its effects on osteoclast formation, cells were cultured in osteoclastogenic medium with varying doses of SPC (0, 0.25, 0.50, or 1.00 mM) for 5 days or 1.00mM SPC for 0, 1, 3, or 5 days. To explore its effects of SPC on osteoclast function, cells were cultured for 5 days until mature osteoclasts formed and subsequently treated with indicated doses of SPC for another 48h.

To evaluate the effects of SPC on osteogenic differentiation, osteoblasts were cultured in

6-well plates in osteoinductive medium supplemented with varying concentrations of SPC (0, 0.25, 0.50, or 1.00 mM) for 7 or 14 days.

To investigate the effects of SPC on Ti-induced inflammation, BMMs were cultured in 6-well plates with complete medium containing 30ng mL^{-1} M-CSF, 0.1mg mL^{-1} Ti particles and varying doses of SPC (0, 0.25, 0.50, or 1.00 mM) for 4h.

Total cellular RNA was extracted according to the manufacturer's instructions using the Qiagen RNeasy Mini kit (Qiagen, Valencia, CA, USA), and total RNA (≤1000ng) was reverse-transcripted into complementary DNA (cDNA) in a 20 μL-reaction volume using a Double-Strand cDNA Synthesis Kit (Takara, Dalian, China). The PCR reaction was performed with 1μL of cDNA as template in triplicates using the Power SYBR® Green PCR Master Mix (Takara) on the ABI StepOnePlus System (Applied Biosystems, Warrington, UK). The cycling conditions were as follows: 95 °C for 30 s and then 40 cycles of 95 °C for 5 s and 60 °C for 30 s. GAPDH was utilized as the housekeeping gene and independent experiments were repeated at least three times. The rat primer sequences were as follows:
GAPDH: forward, 5'-AGG GCT GCC TTC TCT TGT GAC-3'and reverse, 5'-TGG GTA GAA TCA TAC TGG AAC ATG TAG-3';
Cathepsin K: forward, 5'-CCC AGA CTC CAT CGA CTA TCG-3' and reverse, 5'-CTG TAC CCT CTG CAC TTA GCT GCC-3';
TRAP: forward, 5'-GTG CAT GAC GCC AAT GAC AAG-3' and reverse, 5'-TTT CCA GCC AGC ACG TAC CA-3';
NFATc1: forward, 5'-CAG CTG CCG TCG CAC TCT GGT C-3' and reverse, 5'-CCC GGC TGC CTT CCG TCT CAT A-3';
c-Fos: forward, 5'-CAG CCT TTC CTA CTA CCA TTC C-3' and reverse, 5'-ACA GAT CTG CGC AAA AGT CC-3';
dendritic cell-specific transmembrane protein (DC-STAMP): forward, 5'-TTC ATC CAG CAT TTG GGA GT-3' and reverse, 5'-CAT CCA GAC AGC AGA GAG CA-3';
V-ATPase d2: forward, 5'-CAT TTG GCA CTG AAC TGA GC-3' and reverse, 5'-GTC TTC GGC TTG GGC TAAC-3';

iNOS: forward, 5’- AGC GGC CCA TGA CTC TCA-3’ and reverse, 5’- CTG CAC CCA AAC ACC AAG GT-3’;

COX-2: forward, 5’- CCT TGA AGA CGG ACT TGC TCA C-3’ and reverse, 5’- TCT CTC TGC TCT GGT CAA TGG A-3’;

TNF-α: forward, 5’-TAC TCC CAG GTT CTC TTC AAG G-3’ and reverse, 5’-GGA GGC TGA CTT TCT CCT GGT A-3’;

IL-6: forward, 5’-GAG TTG TGC AAT GGC AAT TC-3’ and reverse, 5’-ACT CCA GAA GAC CAG AGC AG-3’;

IL-1β: forward, 5’-GGG CCT CAA GGG GAA GAA TC-3’ and reverse, 5’-ATG TCC CGA CCA TTG CTG TT-3’;

alkaline phosphatase (ALP): forward, 5’-CAC GTT GAC TGT GGT TAC TGC TGA-3’ and reverse, 5’-CCT TGT AAC CAG GCC CGT TG-3’;

Runt-related transcription factor 2 (RUNX2): forward, 5’-GAC TGT GGT TAC CGT CAT GGC-3’ and reverse, 5’-ACT TGG TTT TTC ATA ACA GCG GA-3’;

osteocalcin (OCN): forward, 5’-CCG GCC ACG CTA CTT TCT T-3’ and reverse, 5’-TGG ACT GGA AAC CGT TTC AGA-3’;

sp7: forward, 5’-CAT CTA ACA GGA GGA TTT TGG TTT G-3’ and reverse, 5’-AAG CCT TTG CCC ACC TAC TTT T-3’;

Western blot analysis

To investigate the exact signaling pathway which SPC suppressed, rat BMM cells were seeded into 6-well plates with complete α-MEM containing 30ng mL^{-1} M-CSF for 24 h at a density of 80×10^4/well and subsequently pre-treated with or without 1.00mM SPC for 4h before being stimulated with 50ng mL^{-1} RANKL for 0, 5, 10, 20, 30 or 60 min. In addition, BMMs were seeded at a density of 10×10^4 cells/well were seeded in a 6-well plate with complete α-MEM in the presence of 30ng mL^{-1} M-CSF and 50 ng mL^{-1} RANKL for 0, 1, 3 or 5 days, under treatment with DMSO or 1.00 mM SPC, to examine the effects of SPC on NFATc1 and cathepsin K expression,. To investigate the effects of SPC on Ti-induced expression of iNOS and COX-2, rat BMMs were cultured in 6-well plates at a density of

80×10^4 cells/well in complete α-MEM containing 30ng mL^{-1} M-CSF and different doses of SPC (0, 0.25, 0.50, or 1.00 mM) with or without 0.1 mg mL^{-1} Ti particles for 24h. Additionally, BMMs were seeded into 6-well plates with complete α-MEM containing 30ng mL^{-1} M-CSF for 24 h at a density of 80×10^4 cells/well and were subsequently pre-treated with or without 1.00 mM SPC for 4h before being stimulated with 0.1 mg mL^{-1} Ti particles for 0, 5, 10, 20, 30 or 60 min. Cells were collected and lysed using radioimmunoprecipitation assay (RIPA) buffer (Sangon Biotech Co. Ltd, Shanghai, China) on ice for 30 min, and the lysates were centrifuged at 10,000 rpm for 15 min, followed by the collection of supernatants. Total protein (30μg/lane) was separated on 12% SDS polyacrylamide gels and transferred to PVDF membranes (Millipore, Merck KGaA, Germany). After non-specific blocking with 5% (w/v) BSA-TBS-Tween (TBST) for 1h, membranes were incubated with primary antibodies diluted in TBST containing 5% (w/v) BSA at 4°C overnight. Subsequently, we incubated membranes with the appropriate secondary antibodies at 4°C for 2 hours after rinsing 3 times in PBS, and detected immunoreactive bands with a Bio-Rad XRS chemiluminescence detection system (Bio-Rad, Hercules, CA, USA).

Immunocytochemistry of NF-κB nuclear translocation

BMMs were cultured on cell glass slides in a 24-well plate at a density of 3×10^4/well. BMMs were stimulated with 50ng mL^{-1} RANKL for 10 min, with or without pretreatment with 1.00mM SPC for 4 h, followed by fixation in 4% (w/v) PFA for 30 min at 4 °C. After being permeabilized, and blocked for 30 min in 0.2% (w/v) Triton X-100 and 5% (w/v) BSA at 4 °C, cells were incubated with anti-p65 antibody overnight. BMMs were then incubated with an appropriate fluorescence-conjugated secondary antibody for 2h and stained with DAPI for 10 min. The nuclear translocation of NF-κB was subsequently examined under fluorescence microscopy (Leica)

Establishment of implant loosening model in rats

Titanium (Ti) rods (1.5mm in length and 15mm in diameter) were supplied by the Experimental Research Center of Mechanics, Zhejiang University, and

commercially-available pure Ti particles were obtained from Johnson Matthey (Ward Hill, MA, USA). Ti rods and Ti particles were prepared by baking at 180°C and subsequent mixing with 70% (v/v) ethanol for 48h to remove endotoxin and ensure sterility (Liu *et al.*, 2009). A suspension of Ti particles was prepared as reported previously (Liu *et al.*, 2012a; Bi *et al.*, 2015).

The experimental protocol was designed and performed according to the Guide for the Care and Use of Laboratory Animals promulgated by the United States National Institutes of Health, and was approved by the Animal Care and Use Committee of Zhejiang University. Male adult Sprague-Dawley rats weighing 350g-400g were obtained from the Experimental Animal Center of Zhejiang University. All animals were held in a room at 24±2°C, 60% humidity and 12/12 h light/dark cycle with free access to food and water, with 2 animals per cage. Animals were evaluated daily for signs of pain, distress, or moribundity visually, while their weights were recorded weekly. Animals with such signs or with 10% acute weight loss were euthanized humanely prior to the endpoint. The animal studies were reported in accordance to the ARRIVE guidelines (Kilkenny *et al.*, 2010; McGrath *et al.*, 2015). All efforts were made to minimize the number of utilized animals and animal suffering in this study.

Sixty-six male Sprague-Dawley rats weighing 350g-400g were randomly allocated into 3 groups (n=22 per group): the Ctrl group, the Ti group and the SPC group. Ti particles were used in the Ti group and the SPC group in the surgery, while vehicle was applied in the Ctrl group. After surgery, rats were treated with 20mg kg^{-1} day^{-1} SPC in the SPC group while PBS was administered to the Ctrl and Ti groups. The rat model was established as previously reported (Liu *et al.*, 2012b; Bi *et al.*, 2015). Briefly, rats were anaesthetized with intramuscular xylazine (2 mg kg^{-1}) and ketamine (50 mg kg^{-1}), and bilateral intramedullary Ti rod implantation was performed in distal femurs under aseptic conditions. An implant was inserted into the medullary canal created parallel to the long axis of the femur to achieve a press fit fixation. Before Ti rod insertion, the suspension with 30mg Ti (about 5×10^7 particles) was injected into the canal of rats in the Ti and SPC groups to induce implant loosening while

PBS was injected in the Ctrl group. SPC/PBS was injected intraperitoneally every day after surgery and the body weight of the animals was measured weekly to adjust the drug dosage. Buprenorphine (0.3mg/kg/s. c.) and Carprofen (4mg/kg/p.o.) were administered pre- and post-operation for analgesia, respectively. Penicillin G Procaine (3000U/lb./IM) was injected daily to prevent infection after operation for three days. Thirty mg Ti suspension/PBS was re-injected into the knee joint cavities every other week from the second week postoperatively. Four and twelve weeks after surgery, rats (n=11 per group) were sacrificed with administration of an overdose of pentobarbital (90 mg/kg, Sigma Chemical Co., St. Louis, MO, USA), and specimens were collected for further examination. Six femurs were collected for biomechanical testing and they were wrapped with gauze in normal saline and stored at -20°C at each respective analysis point. The remaining femurs were fixed in 4% (w/v) PFA for bone mineral density (BMD), micro-CT, histological and immunohistochemical analyses. The blood of animals was also collected and serum was stored at -80°C for biochemical analysis (Figure S2A-B).

Peri-implant site BMD measurement

The BMD values of the peri-implant site (n=11 per group) (Figure 5A) were assessed by using dual-energy X-ray absorptionmetry (DEXA; GE Lunar Prodigy, Madison, WI, USA). Femurs were placed with the same position and the area besides the implant was regarded as the region of interests (ROI) for determining the BMD values.

Micro-CT scanning and analysis

Seven femurs from each group at each observation time points were subjected to micro-CT scanning with an isometric resolution of 14.8μm, using a Scanco μCT100 instrument (Scanco Medical, Bassersdorf, Switzerland). Three dimensional (3D) reconstructions of distal femurs were performed with the constrained Gaussian filter (sigma = 1.2, support = 2) to partly suppress the noise in the volumes. A multilevel thresholds procedure (thresholds ranging from 220 to 520) was used to distinguish bone from other tissues and metal in vivo (Gabet *et al.*, 2008).The area at a distance of 500μm from the

surface of implant was regarded as ROI. The parameters of bone trabecula surrounding the implant were quantified and analyzed as previously reported (Bi *et al.*, 2015), including the bone volume / total volume (BV/TV), connective density (Conn.D), structural model index (SMI), trabecular number (Tb.N), trabecular thickness (Tb.Th) and trabecular separation (Tb.Sp).

Biomechanical test of the implant pulling-out strength

A total of thirty femurs (n=6 per group at each observation time) being stored at -20°C, were thawed completely at 4°C overnight before biomechanical testing. Pull-out testing was performed as previously described (Liu *et al.*, 2012a; Bi *et al.*, 2015). Briefly, as shown in Figure 7A, the distal femur with implant inside was fixed vertically in dental cement and positioned on the platform with a canal in the middle. A 1.5mm-diameter indenter was used to push the implant out of the bone cavity with a speed of 1mm min^{-1}, and the maximum fixation strength was recorded by using a Zwick/Roell 2.5 material testing system (Zwick, Ulm, Germany).

Histological and immunohistochemical analysis

After complete decalcification in 10% (w/v) EDTA (pH=7.4), the rods in the remaining specimens were removed and specimens were dehydrated and embedded in paraffin, and then cut into five-micron thick sections. Sections at a distance of 1 mm proximal to the distal femoral growth plate were selected for the histological analysis. Hematoxylin and eosin (H&E), Masson and TRAP stainings were performed on the tissue sections, as previously described (Chen *et al.*, 2015; Zhang *et al.*, 2016b), and specimens were examined and measured under light microscopy (Olympus BX51, Tokyo, Japan). Parameters that were used for histological evaluation of osteolysis around the implant, including bone-implant contact (BIC), ratio of bone area/total area (B.Ar/T.Ar) and mean thickness of the pseudomembrane. The area at a distance of 500 μm from the implant surface was regarded as ROI. Quantitative analysis of the mean thickness of pseudomembrane, BIC and B.Ar/T.Ar were performed in accordance with a previous study (Li *et al.*, 2013). Briefly, B.Ar/T.Ar was measured through

the trabecular area in the visual field /Total area (Figure S3B); BIC was measured through the length of contact perimeter of the implant (green line), with the red line representing the uncontacted portion (Figure S3C); while mean thickness of the pseudomembrane was measured as the total area of the pseudomembrane surrounding the implant/perimeter of the implant (Figure S3D). The quantitative data of TRAP-positive multinucleated osteoclasts formed on the bone surface was collected for each sample.

The levels of NLS-p65 around the implants were analyzed using an immunohistochemistry staining accessory kit (Boshide, Wuhan,China) according to the manufacturer's suggested protocol. At least 5 images (magnification 40×) from the fields at a distance of 300μm from the implant in each section per femur were randomly selected and measured as a means of quantitatively analyzing p65-positive cells. The Image-Pro Plus 6.0 software (Media Cybernetics Inc, Maryland, USA) was utilized for quantification.

Serum Biomarkers

After euthanasia, rat blood (n=10) was collected via the abdominal aorta and centrifuged to separate serum at 2,000 rpm (425xg) for 5 min at 4°C as described previously (Liu *et al.*, 2012a), and then stored at -80°C. Serum CTX-1 level was analyzed according to the manufacturer's protocol using specific ELISA kits. All samples, diluted appropriately, were assayed three times.

Statistical analysis

All data collection and statistical analysis were performed in accordance to the recommendations on experimental design and analysis in Pharmacology (Curtis *et al.*, 2015). All experiments were measured by investigators blind to the treatment. Data were expressed as mean ±SD. Each experiment was repeated at least three times separately and the results were analyzed with SPSS 16.0 software (SPSS, Chicago, IL, USA). An unpaired t-test was used for the comparisons between two groups. One-way ANOVA with *post hoc* Newman-Keuls test was used to analyze differences in multiple comparisons. A probability

level of $p < 0.05$ was considered statistically significant. A post hoc statistical power calculation was performed using G*Power 3.1 software (Dept. of Psychology, Univ Bonn, Germany). The power calculation showed that the differences except the result of B.Ar/T.Ar in 4 weeks can be reliably detected with a power of more than 80%.

Nomenclature of Targets and Ligands

Key protein targets and ligands in this article are hyperlinked to corresponding entries in http://www.guidetopharmacology.org, the common portal for data from the IUPHAR/BPS Guide to PHARMACOLOGY (Southan *et al.*, 2016), and are permanently archived in the Concise Guide to PHARMACOLOGY 2017/18(Alexander *et al.*, 2017).

Results

SPC suppresses RANKL-induced osteoclastogenesis of rat BMMs with negligible cytotoxicity

As shown in Figure S1, flow cytometry results revealed that more than 90% of cells were CD11b positive cells among the whole cell population after 2 days culture in the complete medium with M-CSF. To assess the cytotoxicity of the compound, BMMs were exposed to varying doses of SPC ranging from 0 to 2mM for 48h and 96h. No toxic effects of SPC were found up to the maximal concentration (Figure 1B). BMMs were then cultured with 30ng mL^{-1} M-CSF and 50ng mL^{-1} RANKL with different doses of SPC (0.25, 0.5 and 1 mM) or DMSO of same volume. Dose-dependent suppression of osteoclast formation was confirmed, as indicated by the decreasing number of and area occupied by TRAP-positive multinucleated cells (Figure 1C-E). Moreover, TRAP-positive osteoclasts began to fuse and form after two-day RANKL treatment of the control, whereas significant inhibition of osteoclast differentiation was observed upon treatment with 1mM SPC (Figure 1F-H).

To investigate which stage of osteoclastogenesis that SPC impaired, cells were treated with 1mM SPC at day1-day3 of RANKL stimulation (early stage), day3-day5 (late stage), or day1-day5 (early + late stage). As reported, BMMs proliferate in the early stage, and fuse with one another, forming a multinuclear cell in the late stage (Ikeda *et al.*, 2016). As shown

in Figure 1I-K, a small but marked reduction in the number and size of osteoclasts were observed with early-stage SPC administration. However, no difference was found between the control group and late-stage SPC administration. In the early+late stage SPC administration group, a significant decrease in the size and number of osteoclasts were observed. Collectively, these data confirmed the effects of SPC on inhibiting osteoclast differentiation with negligible cytotoxicity, specific to the early stage and the entire period of RANKL stimulation.

SPC attenuates the formation of F-actin ring and bone resorption in vitro

To further investigate the effects of SPC on osteoclast function, we investigated whether SPC could suppress formation of F-actins, which is generally regarded as a prerequisite for osteoclast bone resorption (Wilson *et al.*, 2009). As shown in Figure 2A, a characteristic F-actin ring formed in osteoclasts without SPC treatment, as visualized by phalloidin-Alexa Fluor 647 staining. In contrast, the sizes of F-actin rings were reduced and more pleomorphic F-actin rings appeared under SPC treatment in a dose-dependent manner (Figure 2C).

With DMSO or different SPC concentrations, mature osteoclasts were next cultured on bone slices to perform an osteoclastic bone resorption assay. In the end, we detected large bone resorption pits on the bone surface by SEM analysis in the group without SPC treatment (Figure 2B). Nevertheless, the resorption area was reduced in a dose-dependent manner upon treatment with 0.25, 0.5 and 1 mM SPC, as compared to the control group (Figure 2D). Therefore, these findings suggested that SPC reduced osteoclastic bone resorption in vitro.

SPC downregulates osteoclast-specific gene expression levels in vitro

To further clarify the role of SPC on osteoclast differentiation and function, we utilized quantitative PCR (qPCR) to examine mRNA expression levels of osteoclast-specific genes, which are generally up-regulated during the process of osteoclastogenesis (Boyle *et al.*, 2003). The data indicated that the mRNA expression levels of several markers of osteoclast differentiation, including Cathepsin K, TRAP, NFATc1, c-Fos, DC-STAMP and V-ATPase d2, were all significantly upregulated upon induction by RANKL during the osteoclast

differentiation process. However, obvious dose- and time-dependent suppressions were observed since day 3 in the groups with SPC treatment during osteoclastogenesis (Figure 3A-B). Moreover, the mRNA expression levels of Cathepsin K, TRAP and V-ATPase d2, which are crucial for mature osteoclast functions, were also inhibited after 48h of SPC treatment in mature osteoclasts (Figure 3C).

SPC inhibits rat osteoclast formation by suppressing activation of the NF-κB signaling pathway without affecting MAPK signaling pathways in vitro

We next utilized Western Blot to explore the exact mechanism by which SPC inhibits osteoclastogenesis. Since the NF-κB and MAPK signaling pathways are recognized as the main signaling mechanisms in osteoclastogenesis (Boyle *et al.*, 2003; Stevenson *et al.*, 2011), we investigated further to confirm whether SPC suppressed osteoclast formation through these two signaling pathways. Upon RANKL stimulation, the phosphorylation of p65, ERK1/2, JNK1/2 and p38 in BMMs were elevated. However, in the SPC treated group (1 mM), there was an increase in p65 phosphorylation after 5 and 10 min stimulation with RANKL, but not to the same extent as RANKL alone, whereas no inhibition was observed in the phosphorylation of ERK1/2, JNK1/2 and p38 (Figure 4A-B, Figure S4A-C). The results thus showed that SPC impaired the NF-κB signaling pathway rather than the MAPK signaling pathway.

To elucidate the mechanism by which SPC inhibited osteoclastolgenesis through NF-κB signaling, we explored the cascade of signaling proteins related to the pathway. In canonical NF-κB signaling associated with osteoclast formation, activation of RANK results in the phosphorylation of the IκB kinase (IKK) complex, which could promote the phosphorylation and degradation of IκBα downstream, leading to phosphorylation and nuclear translocation of p65, which then initiates activation of the downstream pathway (Yu *et al.*, 2014). As shown in Figure 4C-F, we found that the phosphorylation of IκBα and IKK were downregulated by SPC treatment, as well as observed inhibition of degradation of IκBα. To confirm the exact molecular target of SPC, we explored its effect on the upstream regulatory factor TAK1. Interestingly, no change was observed when BMMs were incubated with RANKL or RANKL

combined with SPC (Figure 4G-H), showing that IKKs might be the targets of SPC. Moreover, immunofluorescence staining revealed that the RANKL-induced nuclear translocation of p65 was blocked upon pretreatment with SPC (Figure 4I).

NFATc1, the downstream transcription factor of NF-κB signaling, serves as the master regulator of osteoclastogenesis (Yamashita *et al.*, 2007). It induces the marker gene expression of mature osteoclasts, such as cathepsin K and TRAP. In our study, we found that protein expression levels of NFATc1 and Cathepsin K increased in a time-dependent manner at 1, 3 and 5 days in the presence of RANKL. However, SPC treatment strongly inhibited the elevation of protein expression levels of NFATc1 and Cathepsin K (Figure 4J-L). Consequently, SPC inhibited rat osteoclastogenesis through the NF-κB signaling pathway.

SPC has no effects on the osteogenic differentiation of rat primary osteoblasts

As suppression of the NF-κB signaling pathway was previously reported to upregulate osteoblast differentiation (Novack, 2011), we next investigated the effects of SPC on the osteogenic differentiation of rat primary osteoblasts. No cytotoxicity of SPC was detected in osteoblasts up to 1 mM (Figure S5A). As shown in Figure S2B-C, no differences were observed between osteoblasts treated with osteoinductive medium in the presence of 0, 0.25mM, 0.50mM or 1.00 mM SPC, as shown by ALP staining at 7 days and ARS staining at 14 days (Figure S5B-C). The unchanged mRNA expression levels of *ALP, sp7, RUNX2 and OCN* in each group on day 14 further confirmed the previous observation (Figure S5D).

Administration of SPC inhibits implant loosening in a rat femoral model

To investigate the effects of SPC on wear-particle implant loosening, we utilized a rat femoral model. The administration of 20 mg kg^{-1} SPC daily was found to have the beneficial effect of preventing inflammation in rats (Yifeng *et al.*, 2011). Therefore this dose was utilized for subsequent experiments. As shown in Figure S6, significant reduction in body weight was found in the Ti group from week 5 to the end, as compared with the control group. Comparable increase in body weights were observed in the SPC group relative to the Ti group in the last 3 weeks.

Bilateral femurs were collected and analyzed by iDXA to determine the BMD of the peri-implant bone. The results (Figure 5B) indicated that the BMD of the Ti group was markedly decreased in comparison with the control at 4 weeks and 12 weeks post-surgery. The BMD of the SPC group was higher than that of the Ti group at 12 weeks after administration, but no differences were found at 4 weeks post-surgery.

In order to further confirm the protective effects of SPC on particle-induced bone loss, specimens were analyzed by micro-CT imaging and histological staining. According to 3D reconstruction of micro-CT images, peri-implant bone loss was detected in the Ti group at 4 and 12 weeks post-surgery, when compared to the control group. However, bone resorption in the SPC group was considerably lower than that in the Ti group (Figure 6A, D) at both time points. Quantification of bone parameters presented as BV/TV, Conn.D, SMI, Tb.N, Tb.Sp and Tb.Th confirmed the beneficial effects of SPC in suppressing bone loss (Figure 6G). Notably, peri-implant bone mass of the group with long-term SPC administration (12 weeks) demonstrated the high efficacy of SPC in preventing bone loss. Histological assessment (Figure 6B, C, E, F) showed that the presence of Ti particles led to abnormal structure at the bone-implant interface, with increased pseudomembrane and reduction of bone-implant contact at 4 weeks and 12 weeks post-surgery. However, contemporaneous rats in the SPC group attenuated the formation of pseudomembrane and improved the bone-implant contact. The quantitative histomorphometry analysis supported these findings (Figure 6H). At 4 weeks post-surgery, the Ti group exhibited less BIC and thicker pseudomembrane when compared to the control group, whereas SPC treatment significantly enhanced BIC and inhibited pseudomembrane formation. However, there were no significant differences in B.Ar/T.Ar amongst the three groups. At the late stage (12 weeks), lower B.Ar/T.Ar and BIC, as well as thicker pseudomembrane were observed in the Ti group. Nevertheless, supplementation with SPC significantly inhibited peri-implant trabecular loss and formation of interface membrane, as well as improved bone-implant contact, consistent with the iDXA and micro-CT results.

Biomechanical testing was performed to investigate the effects of SPC on maintaining implant stability within the medullary cavity. The outcomes are presented as the maximal fixation strength (Figure 7B). Particle-induced implant loosening resulted in lower maximal

fixation strength in the Ti group, as compared to the control group at 4 and 12 weeks post-surgery, respectively. However, in the SPC group, the maximal fixation strength improved significantly, compared with that in the Ti group at both 4 and 12 weeks post-surgery.

Administration of SPC suppresses osteoclastogenesis and serum marker of bone resorption in vivo.

TRAP staining and serum analysis were processed at 12 weeks to investigate whether the preventive effect of SPC against implant loosening functioned by inhibiting osteoclast formation and activity at the bone-implant surface. There was observed to be a significantly increased number of multinucleated osteoclasts being formed at the lining of the eroded bone surface in the presence of particles, whereas the number and the size of osteoclasts were significantly reduced upon the application of SPC (Figure 8A, B). Biochemical analysis of the serum bone resorption marker (CTX-1) further confirmed that SPC suppressed osteoclast activity in vivo (Figure 8C).

SPC attenuates implant loosening through NF-κB signaling in vivo

Our in vitro results indicate that SPC downregulates osteoclast formation and bone resorption through suppressing the NF-κB signaling pathway. To further confirm our findings in vivo, we used immunohistochemical staining of activated p65 to investigate the effects of SPC on NF-κB. Our data demonstrated that NF-κB activity in osteoclasts and bone marrow cells surrounding the implant were enhanced by wear particles at 4 weeks and 12 weeks post-surgery. In contrast, the expression of activated p65 was significantly attenuated upon treatment with SPC at both 4 and 12 weeks post-surgery (Figure 8D-E). Hence, the inhibition of implant loosening by SPC was confirmed in vivo.

SPC suppresses Ti-induced inflammation by inhibition of the NF-κB signaling pathway in rat BMMs

The activation of NF-κB signaling by the TLRs/MyD88-dependent pathways in macrophage also plays a role in particle-induced osteolysis through inflammatory activities (Landgraeber *et al.*, 2014). Based on our observation, we next explored the effects of SPC on Ti-induced activation of the NF-κB signaling pathway in BMMs. The Western blot results demonstrated that SPC partly suppressed Ti–induced activation of phosphorylated p65 (Figure S7A, B). Upon further investigating its effects on IκBα and IKK, it was found that SPC was also observed to inhibit the activation of phosphorylated IκBα and IKK, as well as the degradation of IκBα (Figure S7C-F).

To elucidate the effects of SPC on Ti-induced inflammation, we investigated the expression of inflammatory mediators (NO (nitric oxide) and PGE_2) and pro-inflammatory cytokines (Blaine *et al.*, 1997; Hukkanen *et al.*, 1997). As shown in Figure S8A, the production of NO and PGE_2 were markedly increased after administration of Ti, while SPC successfully reduced their production in a dose-dependent manner. COX-2 and iNOS have been reported to be the key enzymes responsible for the production of NO and PGE_2. Hence, we analyzed the expression of COX-2 and iNOS. The results showed that the Ti-induced elevated mRNA and protein expression levels of COX-2 and iNOS were inhibited by SPC in a concentration-dependent manner (Figure S8B-D). Meanwhile, the effects of SPC on the Ti-induced production of pro-inflammatory cytokines, such as TNF-α, IL-1β and IL-6, were explored using qPCR. Figure S9A-C showed that the increased mRNA expression of TNF-α, IL-6 and IL-1β induced by Ti were suppressed the administration of SPC in a concentration-dependent manner. In summary, SPC might mediate anti-inflammatory activity in Ti-induced rat BMMs via suppression of the NF-κB signaling pathway.

Discussion

Aseptic implant loosening is one of the most common complications of total joint arthroplasty and over-activated and increased osteoclast activity play a crucial role in this disease. In our study, we have exerted for the first time that SPC exhibits

anti-osteoclastogenic and anti-bone resorptive effects by suppressing RANKL-induced activation of NF-κB signaling in vitro. We have also demonstrated the preventive effects of SPC on particle-induced implant loosening in a rat model by inhibiting osteoclast formation, resulting in reduced periprosthetic bone loss, diminished pseudomembrane formation, improved bone-implant contact and reduced bone resorption-related turnover, as well as enhancement in the stability of the implants. Moreover, we further validated that SPC attenuates wear-induced osteolysis by modulating NF-κB signaling in vivo. Therefore, our study provides evidence that SPC may be a novel drug for the prevention and treatment of particle-induced implant loosening.

RANKL plays a critical role in driving osteoclast differentiation and function upon binding to RANK on osteoclast precursors, which subsequently triggers a series of cascade activation of downstream signaling pathways, including the ERK, p38, JNK and NF-κB pathways. NF-κB signaling is vital for osteoclast differentiation, as it has been reported that severe osteopetrosis was observed in the p50/p52 double-knockout mouse by blocking osteoclastogenesis (Iotsova *et al.*, 1997). Upon being activated by RANKL stimulation, the RANK receptor associates its cytoplasmic domain with TNF receptor-associated factor-6 (TRAF6), which further forms a complex with Tak1 and Tak1 binding protein-2 (Tab2) (Lomaga *et al.*, 1999; Bai *et al.*, 2008). The complex then phosphorylates and activates Tak1, which in turn leads to the phosphorylation of IKK (Mizukami *et al.*, 2002). However, in its inactive state, a complex consisting of NF-κB with IκB protein is retained within the cytoplasm (Lee *et al.*, 2003). Upon RANKL stimulation, the two catalytic components of IKK, IKKα and IKKβ, work together, resulting in proteasomal degradation of IκB, which subsequently leads to nuclear translocation of NF-κB p65/RelA to modulate the transcription of genes further downstream (Soysa *et al.*, 2009). In our study, we observed that SPC could suppress the phosphorylation of p65. Further investigation showed that SPC inhibited the phosphorylation of IKK and IκBα, as well as the proteasomal degradation of IκBα. However, there were no significant effects of SPC on RANKL-induced activation of TAK1. These data thus indicate that IKKs might be the molecular targets of SPC. Moreover, the immunofluorescence staining confirmed the inhibitory effects of SPC on the nuclear

translocation of p65 in vitro. Immunohistochemistry of activated p65 around the implants revealed the inhibition of NF-κB by SPC in vivo. However, no influence of SPC administration was observed on the phosphorylation of the MAPK signaling pathway.

NFATc1 is identified as the key molecular target of the NF-κB signaling pathway for modulating terminal osteoclastogenic differentiation (Yamashita *et al.*, 2007). The NF-κB proteins are bind to the NFATc1 promoter after nuclear translocation, resulting in auto-amplification of NFATc1 during osteoclastogenesis. This factor is a major regulator of osteoclast-specific genes and protein expression, including TRAP, Cathepsin K, DC-STAMP, and VATPase d2. We demonstrate that SPC attenuates the expression levels of these genes at the mRNA and protein levels, as well as osteoclast differentiation and bone resorption.

To our knowledge, osteoclast is regarded as primary reason causing implant loosening. We then established a rat model of titanium particle-induced implant loosening in distal femurs, which serves as one of the classical experimental models of prosthesis loosening (Liu *et al.*, 2012a; Liu *et al.*, 2012b; Bi *et al.*, 2015). Local distribution of particles around the implants have been reported to diminish weight gain due to inflammation (Liu *et al.*, 2012a). Thick fibrous pseudomembrane, containing wear particles, are usually observed between loose implants and cortical or cancellous bone, which is the result of a variable lymphocyte reaction (Bauer *et al.*, 1999b; Bauer *et al.*, 1999a; Athanasou, 2007), resulting in the increase of osteoclast formation and activation of bone resorption, thus eventually leading to the reduction of implant fixation. Many studies have previously reported that SPC exerts anti-inflammatory activity in vivo with different disease models (Gao *et al.*, 2009; Song *et al.*, 2015; Wang *et al.*, 2016), but no one has yet investigated its pharmacological effects on aseptic loosening. Our results demonstrated the inhibitory effects of SPC on the diminishment of titanium particle-induced weight gain, which may be effected by its anti-inflammatory effects. IDXA and Micro-CT revealed the protective effects of SPC on wear particles-induced periprosthetic bone loss in vivo. Histological data of H&E and Masson staining further confirmed its effects on suppressing bone loss and pseudomembrane formation, as well as improving bone-implant contact. As previously observed in similar models (Smith *et al.*, 2010; Liu *et al.*, 2012b), fixation strength of femoral implants were

significantly reduced due to aseptic loosening induced by intraarticular administration of wear debris, whereas administration of SPC successfully inhibited the fixation reduction. Moreover, TRAP staining confirmed the inhibitory effect of SPC on osteoclastogenesis in vivo. Since wear-induced peri-implant osteolysis is a long-term process of net bone resorption that precedes aseptic loosening in the clinic, we chose specimen of 12-weeks SPC administration for the observation of osteoclasts. Elevated levels of serum CTX-1, a biomarker of bone resorption, have been reported in patients with loosened implants, as compared to those with stable implants (Wilkinson *et al.*, 2003; Streich *et al.*, 2009), which corroborates our results. Moreover, we found that elevated levels of serum CTX-1 were reduced by SPC. Our results thus provide evidence that SPC could prevent peri-implant bone loss and aseptic implant loosening through inhibiting the activation of osteoclasts and bone resorption in vivo.

The NF-κF signaling pathway is crucial in inflammation and wear debris could induce local inflammation by stimulating the release of inflammatory cyteokines in macrophages (Ingham *et al.*, 2005; Landgraeber *et al.*, 2014). When metallic wear particles activate TLR4, adaptor molecules MyD88, IL-1 receptor-associated kinase (IRAK)1, IRAK2, IRAK4 and TRAF6 participate in following reactions, resulting in the activation of the NF-κB signaling pathway and the production of proinflammatory cytokines and inflammatory mediators(Hirayama *et al.*, 2011). Our results showed that SPC inhibited the Ti-induced activation of the NF-κB signaling pathway, and further suppressed the expression of NO, PGE_2, iNOS, COX-2, TNF-α, IL-1β and IL-6,

Nevertheless, there are still some limitations to this study. Ultra-high molecular weight polyethylene (UHMWPE) wear particles were a more common cause of total joint arthroplasty failure than metal particles (Hirakawa *et al.*, 1996). However, metal particles are still a causative factor of implant loosening, and both metal particles and UHMWPE particles could induce osteoclastogenesis and osteolysis in vivo. Therefore, it is reasonable to utilize Ti particles in animal model establishment, even though UHMWPE particles would be more closely related to the clinical scenario. Since the statistical power value for B.Ar/T.Ar in the

4-week samples is lower than 80%, it might be response for the reason that no differences were detected between different groups in the results of B.Ar/T.Ar in the 4 weeks. However, as reliable differences on the BV/TV results of Micro-CT in 4-week samples and B.Ar/T.Ar results of histology in the 12-week samples were detected, we have not increased the number of animals for histology.

Collectively, our study shows SPC exerts an inhibitory effect on osteoclast formation and function by suppressing NF-κB signaling in vitro. We also show its positive efficacy in preventing particle-induced prosthesis loosening and facilitate the maintenance of prosthesis stability in a rat model. Moreover, the effect of SPC on NF-κB signaling is confirmed in vivo. Therefore, we can conclude that SPC may be a novel therapeutic agent for preventing prosthesis loosening and osteoclastic diseases.

Conflict of interest

The authors have declared no conflict of interest.

Author contributions

Shi-gui Yan, Wei-liang Shen and Chen-he Zhou designed this study. Chen-he Zhou and Jia-hong Meng, Zhong-li Shi and Bin Hu performed most of the experiments. Yu-te Yang, Shuai Jiang and Han-xiao Zhu performed some of the molecular cell experiments. Chen-he Zhou, Ze-xin Chen, Chen-chen Zhao, Hao-bo Wu and Wei Yu performed the statistics analysis. Virginia-Jeni Akila Parkman and Boon Chin Heng gave helpful suggestions on the manuscript. Experiments were performed under the supervision of Shi-gui Yan and Wei-liang Shen. Chen-he Zhou wrote the manuscript.

Acknowledgements

This study was supported by research grants from the National Natural Science Foundation of China (81371954, 81472113, 81401785, 81572157). We thank Dr. Mengrui Wu and Dr. Pei Ying Ng from the Harvard School of Dental Medicine, and Dr. An Qin from the Department of Orthopaedics, Ninth People's Hospital, Shanghai Jiao Tong University School of Medicine for technical help and advice.

Reference

Alexander SP, Fabbro D, Kelly E, Marrion NV, Peters JA, Faccenda E*, et al.* (2017). THE CONCISE GUIDE TO PHARMACOLOGY 2017/18: Enzymes. *British journal of pharmacology* **174 Suppl 1:** S272-S359.

Athanasou NA (2007). Peri-implant pathology--relation to implant failure and tumor formation. *Journal of long-term effects of medical implants* **17**(3)**:** 193-206.

Athanasou NA (2016). The pathobiology and pathology of aseptic implant failure. *Bone & joint research* **5**(5)**:** 162-168.

Bai S, Zha JK, Zhao HB, Ross FP, Teitelbaum SL (2008). Tumor Necrosis Factor Receptor-associated Factor 6 Is an Intranuclear Transcriptional Coactivator in Osteoclasts. *Journal of Biological Chemistry* **283**(45)**:** 30861-30867.

Bauer TW, Schils J (1999a). The pathology of total joint arthroplasty. I. Mechanisms of implant fixation. *Skeletal radiology* **28**(8)**:** 423-432.

Bauer TW, Schils J (1999b). The pathology of total joint arthroplasty.II. Mechanisms of implant failure. *Skeletal radiology* **28**(9)**:** 483-497.

Bi F, Shi Z, Zhou C, Liu A, Shen Y, Yan S (2015). Intermittent Administration of Parathyroid Hormone [1-34] Prevents Particle-Induced Periprosthetic Osteolysis in a Rat Model. *PloS one* **10**(10)**:** e0139793.

Blaine TA, Pollice PF, Rosier RN, Reynolds PR, Puzas JE, O'Keefe RJ (1997). Modulation of the production of cytokines in titanium-stimulated human peripheral blood monocytes by pharmacological agents. The role of cAMP-mediated signaling mechanisms. *The Journal of bone and joint surgery. American volume* **79**(10)**:** 1519-1528.

Boyle WJ, Simonet WS, Lacey DL (2003). Osteoclast differentiation and activation. *Nature* **423**(6937)**:** 337-342.

Chen S, Jin G, Huang KM, Ma JJ, Wang Q, Ma Y*, et al.* (2015). Lycorine suppresses RANKL-induced osteoclastogenesis in vitro and prevents ovariectomy-induced osteoporosis and titanium particle-induced osteolysis in vivo. *Scientific reports* **5:** 12853.

Curtis MJ, Bond RA, Spina D, Ahluwalia A, Alexander SP, Giembycz MA*, et al.* (2015). Experimental design and analysis and their reporting: new guidance for publication in BJP. *British journal of pharmacology* **172**(14)**:** 3461-3471.

Gabet Y, Kohavi D, Kohler T, Baras M, Muller R, Bab I (2008). Trabecular bone gradient in rat long bone metaphyses: mathematical modeling and application to morphometric measurements and correction of implant positioning. *Journal of bone and mineral research : the official journal of the American Society for Bone and Mineral Research* **23**(1)**:** 48-57.

Gallo J, Vaculova J, Goodman SB, Konttinen YT, Thyssen JP (2014). Contributions of human tissue analysis to understanding the mechanisms of loosening and osteolysis in total hip replacement. *Acta biomaterialia* **10**(6)**:** 2354-2366.

Gao Y, Jiang W, Dong C, Li C, Fu X, Min L*, et al.* (2012). Anti-inflammatory effects of sophocarpine in LPS-induced RAW 264.7 cells via NF-kappaB and MAPKs signaling pathways. *Toxicology in vitro : an international journal published in association with BIBRA* **26**(1)**:** 1-6.

Gao Y, Li G, Li C, Zhu X, Li M, Fu C*, et al.* (2009). Anti-nociceptive and anti-inflammatory activity of sophocarpine. *Journal of ethnopharmacology* **125**(2)**:** 324-329.

Hirakawa K, Bauer TW, Stulberg BN, Wilde AH (1996). Comparison and quantitation of wear debris of failed total hip and total knee arthroplasty. *Journal of biomedical materials research* **31**(2)**:** 257-263.

Hirayama T, Tamaki Y, Takakubo Y, Iwazaki K, Sasaki K, Ogino T*, et al.* (2011). Toll-like receptors and their adaptors are regulated in macrophages after phagocytosis of lipopolysaccharide-coated titanium particles. *Journal of orthopaedic research : official publication of the Orthopaedic Research Society* **29**(7)**:** 984-992.

Holt G, Murnaghan C, Reilly J, Meek RM (2007). The biology of aseptic osteolysis. *Clinical orthopaedics and related research* **460:** 240-252.

Hukkanen M, Corbett SA, Batten J, Konttinen YT, McCarthy ID, Maclouf J*, et al.* (1997). Aseptic loosening of total hip replacement. Macrophage expression of inducible nitric oxide synthase and cyclo-oxygenase-2, together with peroxynitrite formation, as a possible mechanism for early prosthesis failure. *The Journal of bone and joint surgery. British volume* **79**(3)**:** 467-474.

Ikeda K, Takeshita S (2016). The role of osteoclast differentiation and function in skeletal homeostasis. *Journal of biochemistry* **159**(1)**:** 1-8.

Ingham E, Fisher J (2005). The role of macrophages in osteolysis of total joint replacement. *Biomaterials* **26**(11)**:** 1271-1286.

Iotsova V, Caamano J, Loy J, Yang Y, Lewin A, Bravo R (1997). Osteopetrosis in mice lacking NF-kappaB1 and NF-kappaB2. *Nat Med* **3**(11)**:** 1285-1289.

Jiang Y, Jia T, Wooley PH, Yang SY (2013). Current research in the pathogenesis of aseptic implant loosening associated with particulate wear debris. *Acta orthopaedica Belgica* **79**(1)**:** 1-9.

Jurdic P, Saltel F, Chabadel A, Destaing O (2006). Podosome and sealing zone: specificity of the osteoclast model. *European journal of cell biology* **85**(3-4)**:** 195-202.

Kilkenny C, Browne W, Cuthill IC, Emerson M, Altman DG, Group NCRRGW (2010). Animal research: reporting in

vivo experiments: the ARRIVE guidelines. *British journal of pharmacology* **160**(7)**:** 1577-1579.

Kong YY, Feige U, Sarosi I, Bolon B, Tafuri A, Morony S*, et al.* (1999). Activated T cells regulate bone loss and joint destruction in adjuvant arthritis through osteoprotegerin ligand. *Nature* **402**(6759)**:** 304-309.

Landgraeber S, Jager M, Jacobs JJ, Hallab NJ (2014). The pathology of orthopedic implant failure is mediated by innate immune system cytokines. *Mediators of inflammation* **2014:** 185150.

Lee ZH, Kim HH (2003). Signal transduction by receptor activator of nuclear factor kappa B in osteoclasts. *Biochemical and biophysical research communications* **305**(2)**:** 211-214.

Li C, Gao Y, Tian J, Shen J, Xing Y, Liu Z (2011). Sophocarpine administration preserves myocardial function from ischemia-reperfusion in rats via NF-kappaB inactivation. *Journal of ethnopharmacology* **135**(3)**:** 620-625.

Li J, Li L, Chu H, Sun X, Ge Z (2014). Oral sophocarpine protects rat heart against pressure overload-induced cardiac fibrosis. *Pharmaceutical biology* **52**(8)**:** 1045-1051.

Li YF, Li XD, Bao CY, Chen QM, Zhang H, Hu J (2013). Promotion of peri-implant bone healing by systemically administered parathyroid hormone (1-34) and zoledronic acid adsorbed onto the implant surface. *Osteoporosis international : a journal established as result of cooperation between the European Foundation for Osteoporosis and the National Osteoporosis Foundation of the USA* **24**(3)**:** 1063-1071.

Liu F, Zhu Z, Mao Y, Liu M, Tang T, Qiu S (2009). Inhibition of titanium particle-induced osteoclastogenesis through inactivation of NFATc1 by VIVIT peptide. *Biomaterials* **30**(9)**:** 1756-1762.

Liu S, Virdi AS, Sena K, Hughes WF, Sumner DR (2012a). Bone turnover markers correlate with implant fixation in a rat model using LPS-doped particles to induced implant loosening. *Journal of biomedical materials research. Part A* **100**(4)**:** 918-928.

Liu S, Virdi AS, Sena K, Sumner DR (2012b). Sclerostin antibody prevents particle-induced implant loosening by stimulating bone formation and inhibiting bone resorption in a rat model. *Arthritis and rheumatism* **64**(12)**:** 4012-4020.

Liu X, Zhu S, Cui J, Shao H, Zhang W, Yang H*, et al.* (2014). Strontium ranelate inhibits titanium-particle-induced osteolysis by restraining inflammatory osteoclastogenesis in vivo. *Acta biomaterialia* **10**(11)**:** 4912-4918.

Lomaga MA, Yeh WC, Sarosi I, Duncan GS, Furlonger C, Ho A*, et al.* (1999). TRAF6 deficiency results in osteopetrosis and defective interleukin-1, CD40, and LPS signaling. *Genes & development* **13**(8)**:** 1015-1024.

McGrath JC, Lilley E (2015). Implementing guidelines on reporting research using animals (ARRIVE etc.): new requirements for publication in BJP. *British journal of pharmacology* **172**(13)**:** 3189-3193.

Mizukami J, Takaesu G, Akatsuka H, Sakurai H, Ninomiya-Tsuji J, Matsumoto K*, et al.* (2002). Receptor activator

of NF-kappaB ligand (RANKL) activates TAK1 mitogen-activated protein kinase kinase kinase through a signaling complex containing RANK, TAB2, and TRAF6. *Molecular and cellular biology* **22**(4)**:** 992-1000.

Novack DV (2011). Role of NF-kappaB in the skeleton. *Cell research* **21**(1)**:** 169-182.

Pajarinen J, Lin TH, Sato T, Yao Z, Goodman S (2014). Interaction of Materials and Biology in Total Joint Replacement - Successes, Challenges and Future Directions. *Journal of materials chemistry. B, Materials for biology and medicine* **2**(41)**:** 7094-7108.

Pearson G, Robinson F, Beers Gibson T, Xu BE, Karandikar M, Berman K*, et al.* (2001). Mitogen-activated protein (MAP) kinase pathways: regulation and physiological functions. *Endocrine reviews* **22**(2)**:** 153-183.

Porter M (2016). National Joint Registry for England, Wales ,Northern Ireland and the Isle of Man: 13th Annual Report.

Purdue PE, Koulouvaris P, Potter HG, Nestor BJ, Sculco TP (2007). The cellular and molecular biology of periprosthetic osteolysis. *Clinical orthopaedics and related research* **454:** 251-261.

Qu SX, Bai YL, Liu XM, Fu R, Duan K, Weng J (2013). Study on in vitro release and cell response to alendronate sodium-loaded ultrahigh molecular weight polyethylene loaded with alendronate sodium wear particles to treat the particles-induced osteolysis. *Journal of Biomedical Materials Research Part A* **101**(2)**:** 394-403.

Smith RA, Maghsoodpour A, Hallab NJ (2010). In vivo response to cross-linked polyethylene and polycarbonate-urethane particles. *Journal of biomedical materials research. Part A* **93**(1)**:** 227-234.

Song CY, Zeng X, Wang Y, Shi J, Qian H, Zhang Y*, et al.* (2015). Sophocarpine attenuates toll-like receptor 4 in steatotic hepatocytes to suppress pro-inflammatory cytokines synthesis. *Journal of gastroenterology and hepatology* **30**(2)**:** 405-412.

Southan C, Sharman JL, Benson HE, Faccenda E, Pawson AJ, Alexander SP*, et al.* (2016). The IUPHAR/BPS Guide to PHARMACOLOGY in 2016: towards curated quantitative interactions between 1300 protein targets and 6000 ligands. *Nucleic acids research* **44**(D1)**:** D1054-1068.

Soysa NS, Alles N (2009). NF-kappaB functions in osteoclasts. *Biochemical and biophysical research communications* **378**(1)**:** 1-5.

Stevenson DA, Schwarz EL, Carey JC, Viskochil DH, Hanson H, Bauer S*, et al.* (2011). Bone resorption in syndromes of the Ras/MAPK pathway. *Clinical genetics* **80**(6)**:** 566-573.

Streich NA, Gotterbarm T, Jung M, Schneider U, Heisel C (2009). Biochemical markers of bone turnover in aseptic loosening in hip arthroplasty. *International orthopaedics* **33**(1)**:** 77-82.

Takaesu G, Ninomiya-Tsuji J, Kishida S, Li X, Stark GR, Matsumoto K (2001). Interleukin-1 (IL-1)

receptor-associated kinase leads to activation of TAK1 by inducing TAB2 translocation in the IL-1 signaling pathway. *Molecular and cellular biology* **21**(7)**:** 2475-2484.

Takahashi N, Udagawa N, Tanaka S, Suda T (2003). Generating murine osteoclasts from bone marrow. *Methods in molecular medicine* **80:** 129-144.

Takayanagi H, Kim S, Koga T, Nishina H, Isshiki M, Yoshida H*, et al.* (2002). Induction and activation of the transcription factor NFATc1 (NFAT2) integrate RANKL signaling in terminal differentiation of osteoclasts. *Developmental cell* **3**(6)**:** 889-901.

Wang D, Xu N, Zhang Z, Yang S, Qiu C, Li C*, et al.* (2016). Sophocarpine displays anti-inflammatory effect via inhibiting TLR4 and TLR4 downstream pathways on LPS-induced mastitis in the mammary gland of mice. *Int Immunopharmacol* **35:** 111-118.

Wang XJ, Deng HZ, Jiang B, Yao H (2012). The natural plant product sophocarpine ameliorates dextran sodium sulfate-induced colitis in mice by regulating cytokine balance. *International journal of colorectal disease* **27**(5)**:** 575-581.

Wilkinson JM, Hamer AJ, Rogers A, Stockley I, Eastell R (2003). Bone mineral density and biochemical markers of bone turnover in aseptic loosening after total hip arthroplasty. *Journal of orthopaedic research : official publication of the Orthopaedic Research Society* **21**(4)**:** 691-696.

Wilson SR, Peters C, Saftig P, Bromme D (2009). Cathepsin K activity-dependent regulation of osteoclast actin ring formation and bone resorption. *The Journal of biological chemistry* **284**(4)**:** 2584-2592.

Yamashita T, Yao Z, Li F, Zhang Q, Badell IR, Schwarz EM*, et al.* (2007). NF-kappaB p50 and p52 regulate receptor activator of NF-kappaB ligand (RANKL) and tumor necrosis factor-induced osteoclast precursor differentiation by activating c-Fos and NFATc1. *The Journal of biological chemistry* **282**(25)**:** 18245-18253.

Yang ZF, Li CZ, Wang W, Chen YM, Zhang Y, Liu YM*, et al.* (2011). Electrophysiological mechanisms of sophocarpine as a potential antiarrhythmic agent. *Acta pharmacologica Sinica* **32**(3)**:** 311-320.

Yifeng M, Bin W, Weiqiao Z, Yongming Q, Bing L, Xiaojie L (2011). Neuroprotective effect of sophocarpine against transient focal cerebral ischemia via down-regulation of the acid-sensing ion channel 1 in rats. *Brain research* **1382:** 245-251.

Yu B, Chang J, Liu Y, Li J, Kevork K, Al-Hezaimi K*, et al.* (2014). Wnt4 signaling prevents skeletal aging and inflammation by inhibiting nuclear factor-kappaB. *Nat Med* **20**(9)**:** 1009-1017.

Zhang PP, Wang PQ, Qiao CP, Zhang Q, Zhang JP, Chen F*, et al.* (2016a). Differentiation therapy of hepatocellular carcinoma by inhibiting the activity of AKT/GSK-3beta/beta-catenin axis and TGF-beta induced EMT with sophocarpine. *Cancer letters* **376**(1)**:** 95-103.

Zhang W, Xue D, Yin H, Wang S, Li C, Chen E*, et al.* (2016b). Overexpression of HSPA1A enhances the osteogenic differentiation of bone marrow mesenchymal stem cells via activation of the Wnt/beta-catenin signaling pathway. *Scientific reports* **6:** 27622.

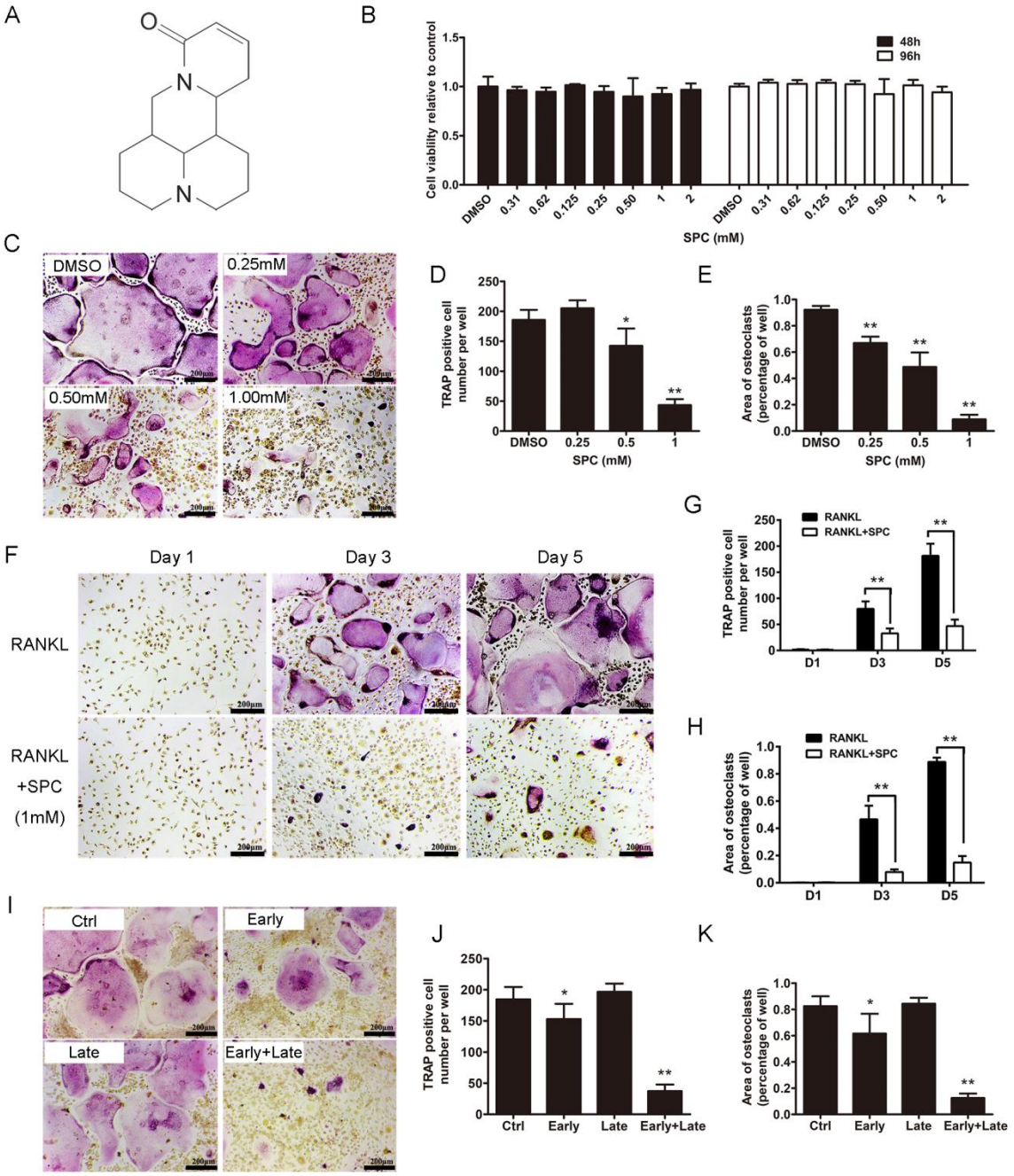

Figure 1

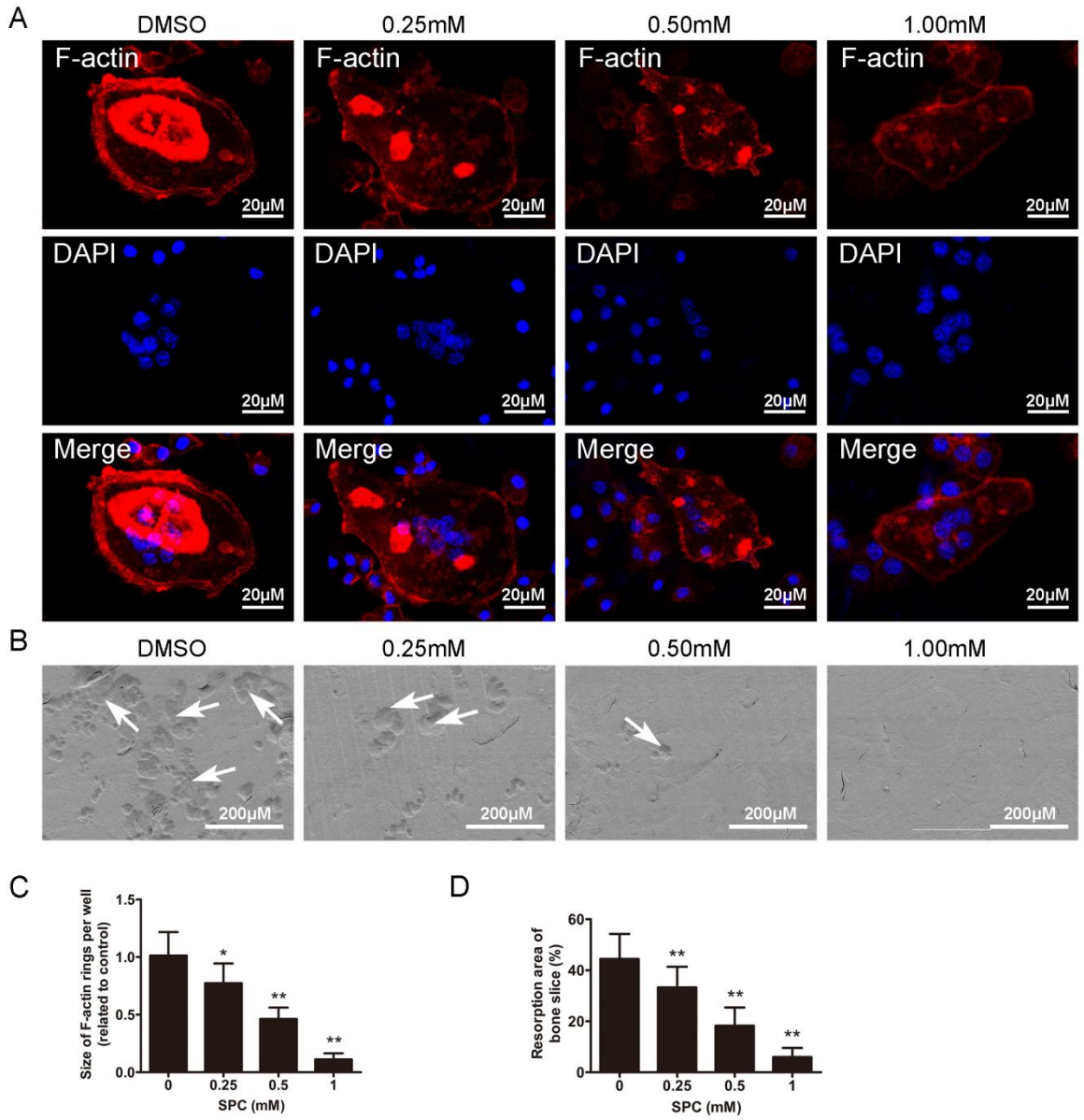

Figure 2

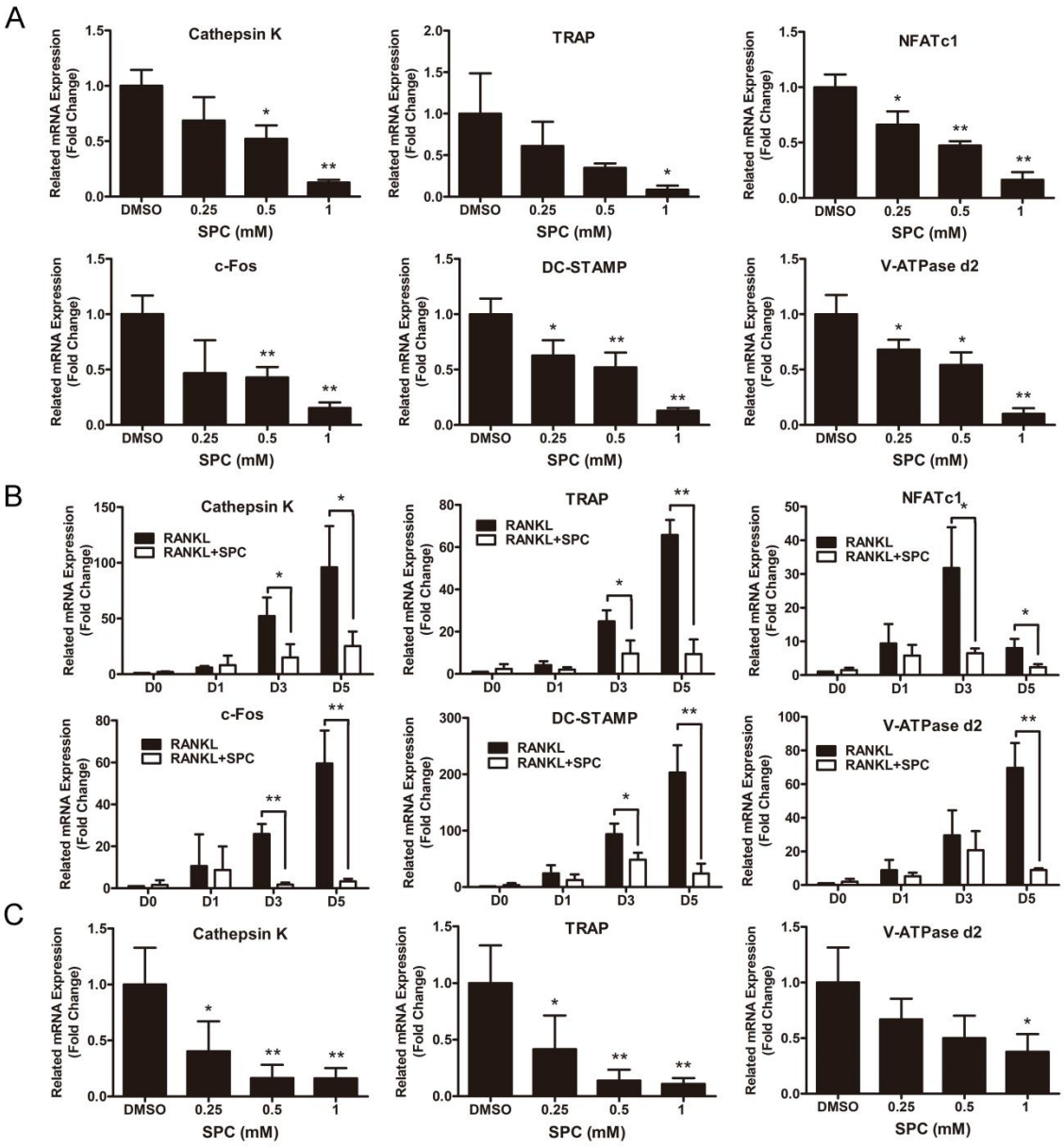

Figure 3

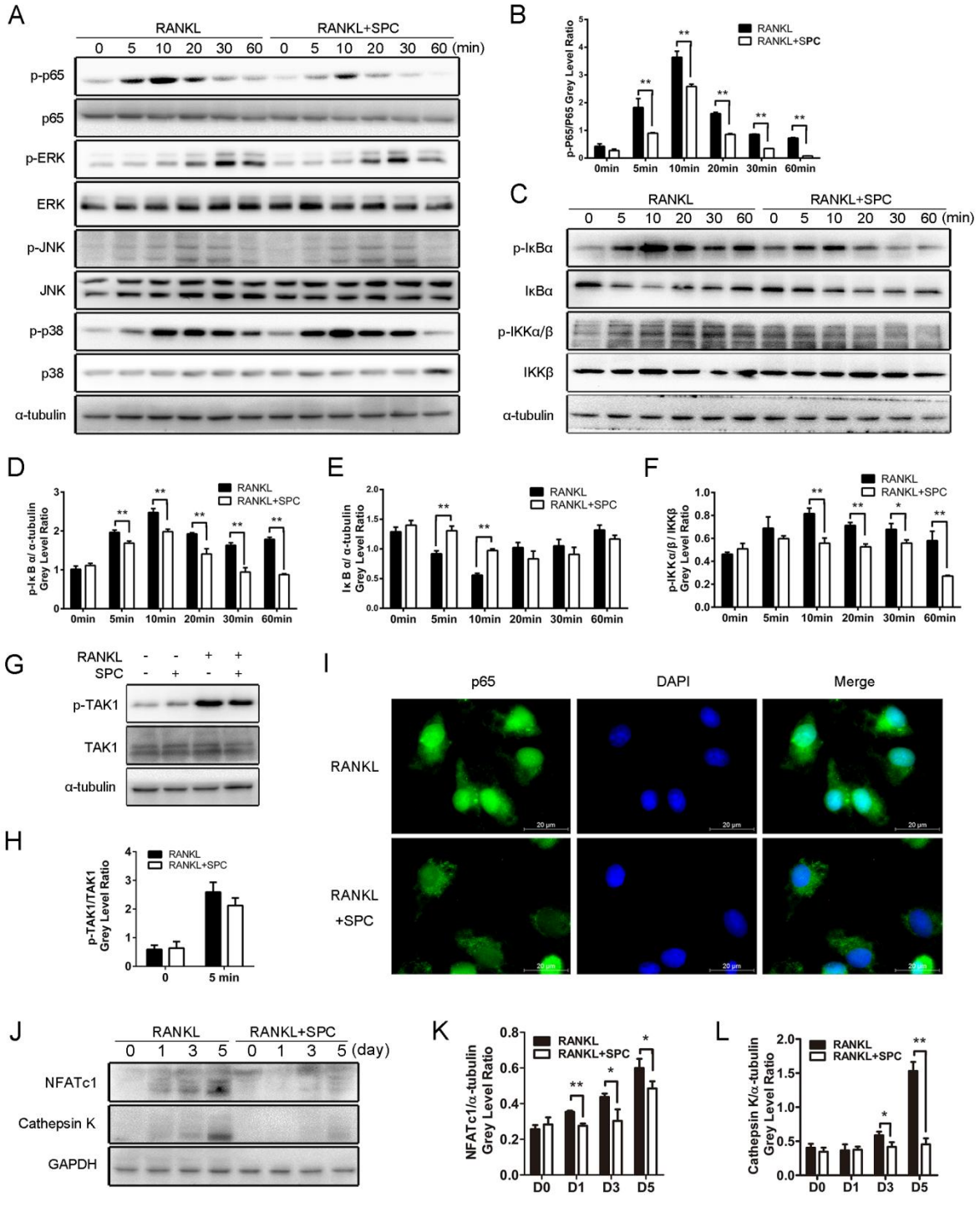

Figure 4

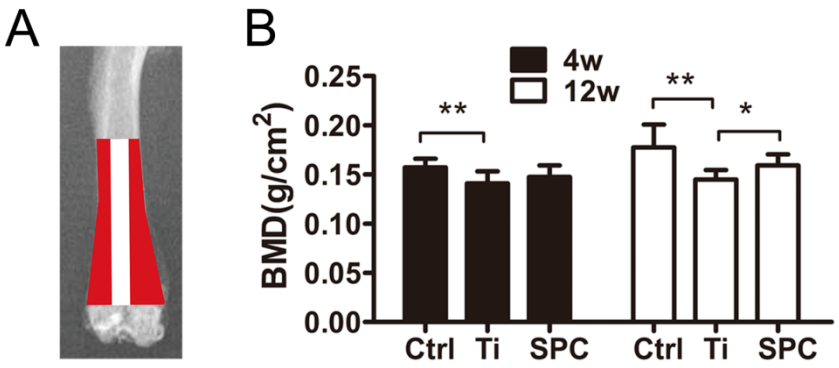

Figure 5

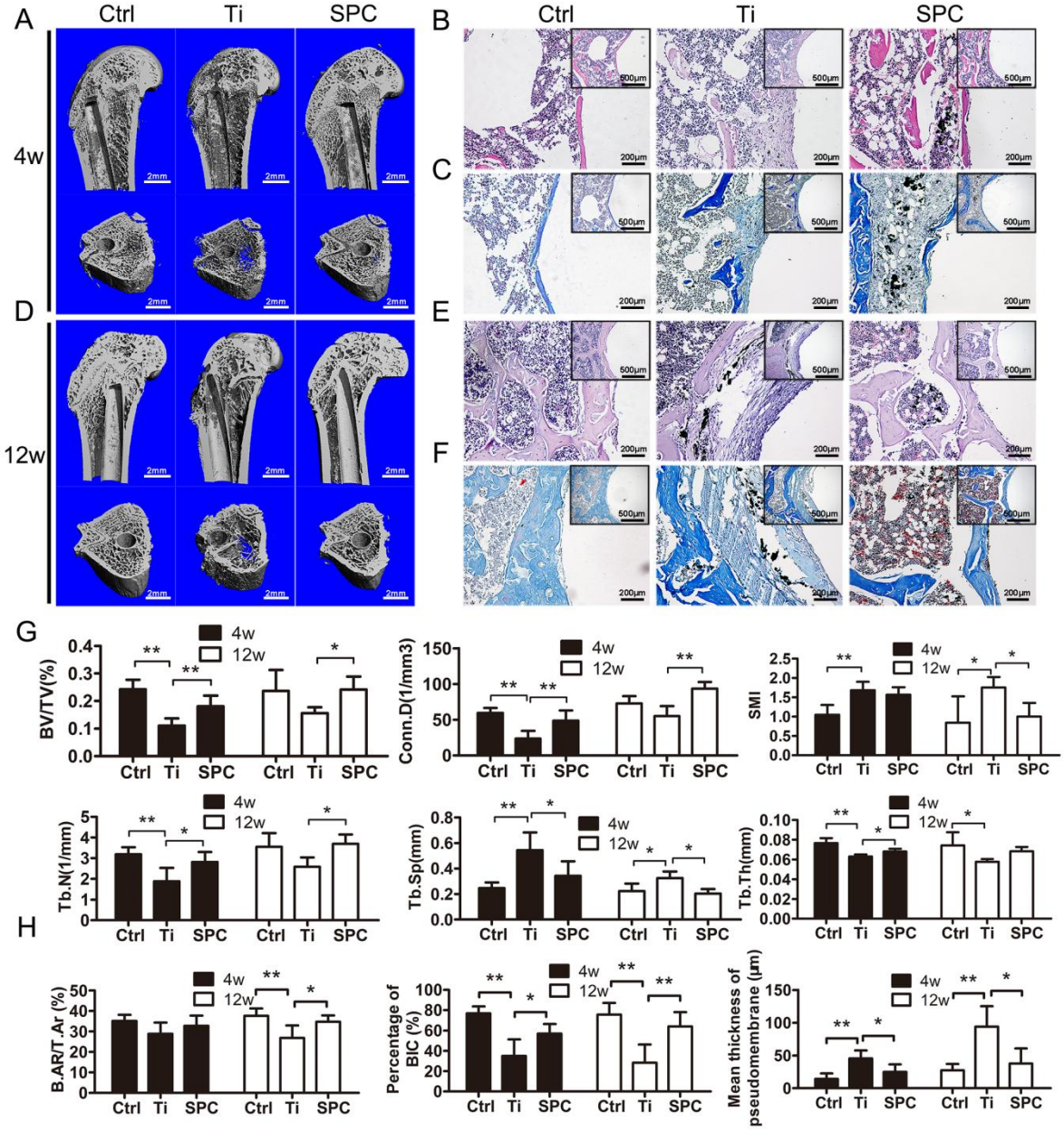

Figure 6

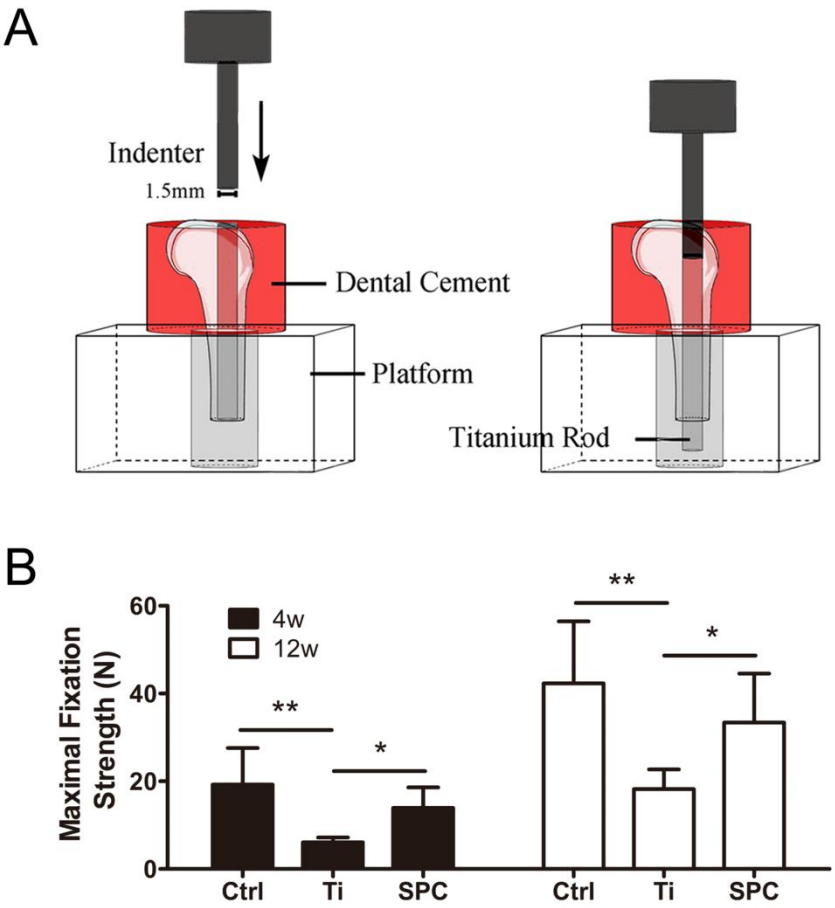

Figure 7

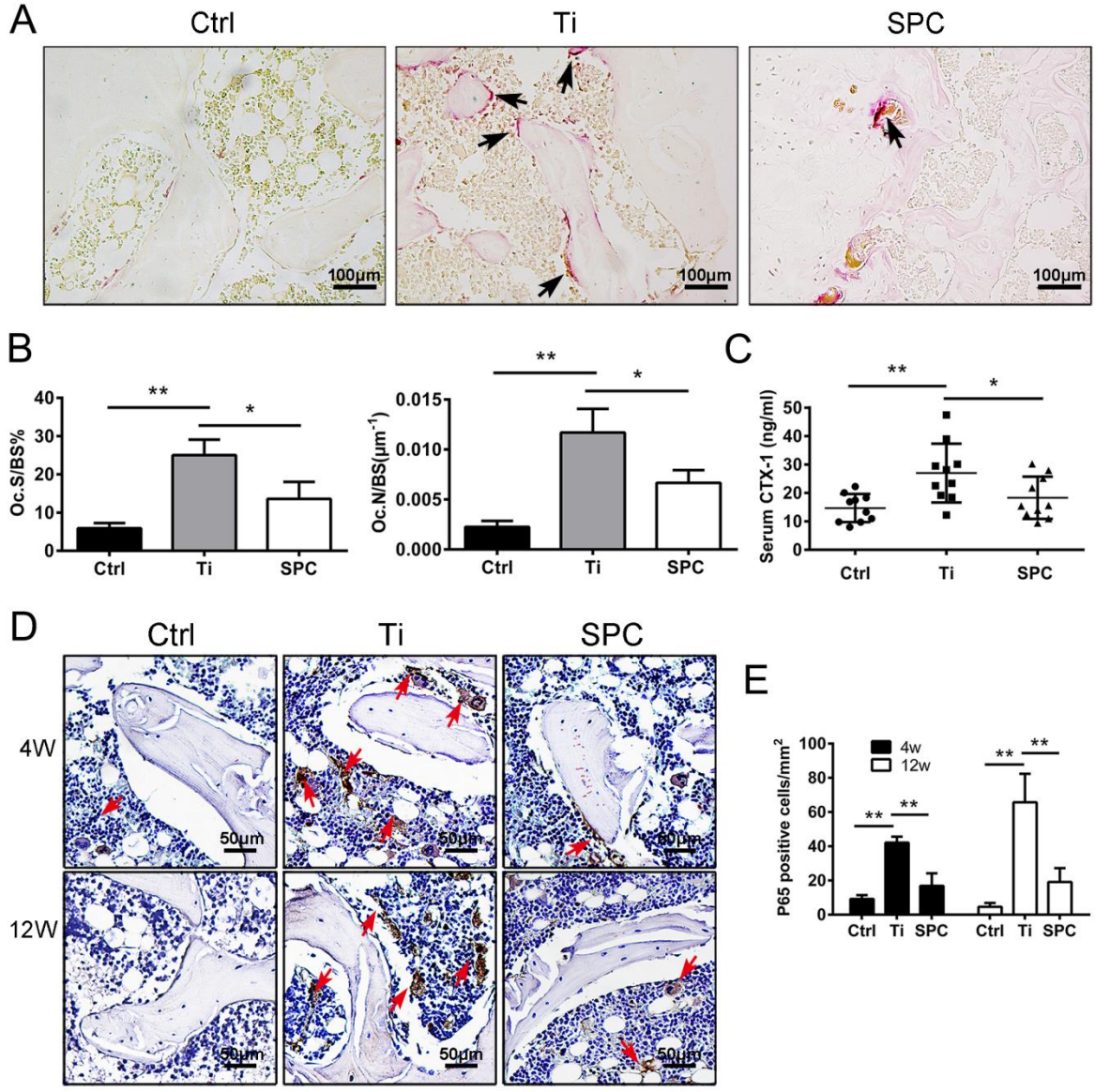

Figure 8